Proceedings of ASME Turbo Expo 2011
GT2011
June 6-10, 2011, Vancouver, British Columbia, Canada

GT2011-46190

STEADY STATE VERSUS TIME-ACCURATE CFD IN AN AUTOMATED AIRFOIL SECTION OPTIMIZATION OF A COUNTER ROTATING FAN STAGE

Georgios Goinis[*], Stefan Stollenwerk, Eberhard Nicke and Edmund Kügeler
German Aerospace Center (DLR)
Institute of Propulsion Technology
Linder Höhe, 51147 Cologne, Germany
Email: georgios.goinis@dlr.de

ABSTRACT

Automated CFD-based optimization procedures have become an essential part of modern aerodynamic compressor design. Although time-accurate CFD provides a higher physical accuracy, due to limited resources still mainly steady state CFD is used. With a constantly growing computing power the question arises, whether it is worth it increasing the computing effort per evaluation using more accurate CFD codes, in order to improve the optimization results.

This work investigates how the results of an automated aerodynamic compressor optimization depend on the simulation procedure used to calculate the flow solutions during the optimization. Two configurations of a counter-rotating fan stage with different axial inter-blade spacing have been optimised using a Q3D approach for the midspan airfoil sections. The configurations were chosen, as to represent the two possibilities of low and high unsteady flow interaction between the blade rows. In each case two automated optimizations have been performed. One based on a steady simulation procedure (RANS), the other on a time-accurate (URANS). In addition, the configuration with low axial spacing has been optimized using a RANS procedure with a determinsitic stress model (RANS-DS).

A dependency of the optimization results on the CFD method used has been observed for cases showing high unsteady interaction between the blade rows. The best optimization results were obtained using a time-accurate URANS CFD-solver. A comparison between RANS and RANS-DS showed an advantage of using RANS-DS.

NOMENCLATURE

$D_{\max}$	maximum thickness [-]
N	time steps per period [-]
T	time per period [s]
Π_{tot}	total pressure ratio [-]
β_1	leading edge angle [°]
β_2	trailing edge angle [°]
β_S	stagger angle [°]
$\dot{m}$	mass flow rate [kg/s]
η_{is}	isentropic efficiency [-]
μ_d	deterministic pseudo-viscosity $[Pa \cdot s]$
τ	stress tensor [N/m^2]
Ma_{ax}	axial Mach-number [-]
c	chord $[m]$
f	fitness function
n	time step [-]
r_{LE}	leading edge radius $[m]$
t	time [s]
$x_{D\max}$	position of maximum thickness [-]
CFD	computational fluid dynamics
DLR	German Aerospace Center
DOE	design of experiment
DS	deterministic stress
DSO	"DS optimization" - based on RANS-DS code
LE	leading edge
OP	operating point
PID	proportional–integral–derivative
Q3D	quasi 3D
R1, R2	rotor one, rotor two

[*]Address all correspondence to this author.

RANS	Reynolds Averaged Navier-Stokes
RANS-DS	RANS solver including DS model
SS	steady state
SSO	"steady state optimization" - based on RANS code
TE	trailing edge
URANS	unsteady Reynolds Averaged Navier-Stokes
US	unsteady
USO	"unsteady optimization" - based on URANS code

INTRODUCTION

The application of optimization methods has become a standard approach in the aerodynamic design of turbomachinery components. Typically the design tools, including the CFD solver, are arranged in a process chain and coupled with optimization algorithms. The optimization algorithms predict promising new designs (referred to as "members" or "individuals") which are then evaluated by executing the process chain. Depending especially on the grid size and CFD solver incorporated, the process chain run time of an evaluation can be significant. The number of possible evaluations during an optimization is therefore often limited by the available computing resources. The designer is then faced with the question on how to use the computing resources in the most efficient way, in order to obtain the best possible optimization results. This consideration involves many aspects, such as the parameterisation of the problem, the computational grid, the type of CFD solver used and solver settings. The decision is always a trade-off between the accuracy of the mathematical problem description and evaluation on the one hand and the achievable state of convergence of the optimization, mainly affected by the number of possible evaluations, on the other.

With a continuously growing computing power and more sophisticated optimization procedures available, the use of time-accurate CFD methods in the framework of optimizations, instead of steady state methods only, is no longer beyond the means. Consequently, when setting up an optimization, the question whether steady state or unsteady CFD (such as RANS and URANS) is used for the evaluation of new geometries is one that has to be asked. However, under the premiss of a limited amount of computing power available the additional computing cost required for time-accurate evaluations will result in a reduced number of evaluations possible for the optimization. As the difference in computing cost can be up to one magnitude, the general practice is to use steady state CFD during the optimization process and to verify the optimization results using time-accurate CFD. This practice often shows that the improvements in fitness function value predicted by the steady state CFD methods are only partially obtained by unsteady CFD calculations (see e.g. [1]). This underlines the question whether better optimization results can be obtained using more sophisticated CFD methods during an optimization, such as URANS instead of RANS.

Comparing different CFD methods during an optimization, this study investigates how the results of an optimization depend on the CFD method used. Three different CFD methods providing a different physical accuracy at different computational costs are compared: URANS, RANS and RANS with a deterministic stress (DS) model (RANS-DS). The main part of the study will focus on the comparison of steady state with time accurate CFD (RANS/URANS). In addition to that a RANS-DS method is investigated. In terms of computational power needed, RANS is the cheapest method and therefore, as already mentioned, commonly used in optimizations. URANS on the other hand is computationally expensive but provides a higher physical accuracy, as no steady state assumption is made. RANS-DS methods have been developed to provide a higher physical accuracy compared to RANS methods by modelling the effect of unsteadiness on the time averaged solution, at only slightly higher computing costs.

All optimizations are based on one of two configurations of the same test case and on the same optimization setup. The test case is presented in the first section of the paper, followed by an explanation of the optimization procedure and the tools used. This includes notes on the automated convergence control used for time-accurate CFD simulations, as well as a brief overview on the deterministic stress approach. Thereafter comparisons of the optimizations based on the different CFD methods are presented. In order to compare Pareto front members of optimizations based on different CFD methods these members have been recalculated using the respective other method. A complete outline of the study is shown in figure 1. At first the comparison of RANS and URANS based optimizations for configuration one, with high axial spacing is discussed. Then the results of identical optimizations but for configuration two are discussed. Finally results of an optimization based on RANS-DS for configuration two are compared to the previous results for the same configuration.

TEST CASE AND NUMERICAL SETUP

As test case for this study, a counter rotating fan configuration has been selected. Key stage design parameters are listed in table 1. To limit the computational resources needed for the study a Q3D-CFD approach for the mid span section of the blades has been used. For the same reason only one operating point has been taken into account for the optimizations.

Two configurations, differing in the the axial spacing between the two rotors, were investigated. The first configuration has a high axial spacing of approximately 2 rotor one axial chord lengths, whereas for the second configuration the axial spacing was reduced by approximately 85% resulting in an axial spacing of approximately 0.3 rotor one axial chord lengths, as shown in figure 2.

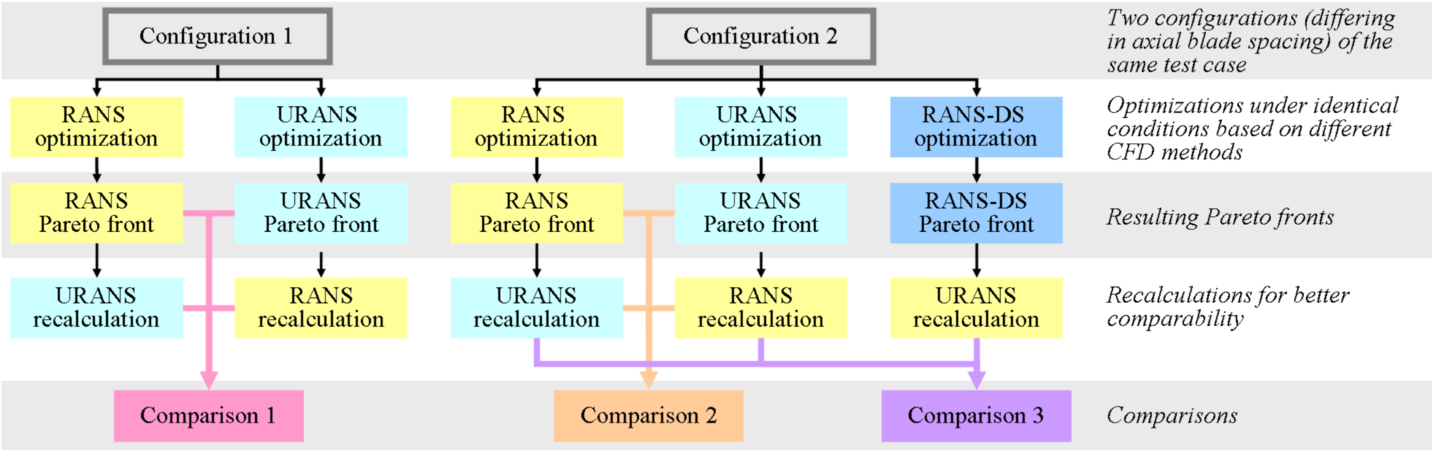

FIGURE 1. OUTLINE OF THE STUDY.

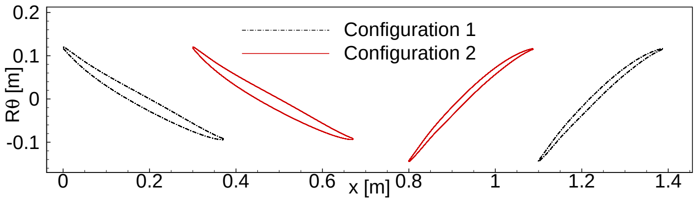

FIGURE 2. COMPARISON OF CONFIGURATION 1 AND 2.

TABLE 1. STAGE DESIGN PARAMETERS

Design parameter	Value
R1 rotational speed u_1 (at LE) [m/s]	-153
R1 blade count [-]	12
R1 space to chord ratio $(t/c)_{R1}$ [-]	1.2
R2 rotational speed u_2 (at LE) [m/s]	117
R2 blade count [-]	8
R2 space to chord ratio $(t/c)_{R1}$ [-]	2.0
Stage total pressure ratio Π_{tot} [-]	1.3

The grid used for the computations consisted of approximately 80000 cells in two radial layers for both configurations (equally good spatial discretization). The grid size is a compromise between grid sensitivity and performance, whereby the grid sensitivity has been checked to be low enough not to distort the results of the study. The stream tube with a non-constant height of $h = f(x)$ has been obtained as a result of a preliminary mean line study and was not changed during the optimizations. A wall-function approach for the calculation of the boundary layer was used, with dimensionless wall distances of $y^+ \approx 50$ on the blade surfaces.

The CFD solver used for the simulations is the Navier-Stokes solver *TRACE*, which is being developed specifically for turbomachinery flows at the DLR Institute of Propulsion Technology. Details on *TRACE* can be found in Ashcroft [2] and Becker [3].

A general sketch of the airfoil parametrisation is given in figure 4. Not all airfoil parameters were selected as free parameters for the optimization but only important, dominant ones (highlighted in green in figure 4). The allowed range for the parameters was chosen to be high, in order not to introduce any limitations due to a too restrictive parameter range. The airfoil optimization parameters and the range of allowed values are shown in table 2. In addition to these parameters four B-spline parameters for the suction side definition as well as an additional leading edge parameter were free to be optimised for each rotor. The pressure surfaces were defined using a thickness distribution. Other parameters were held constant, such as trailing edge radius and axial chord length.

In overall twelve parameters for each rotor were allowed to be modified during the optimization resulting in a total of 24 free parameters.

OPTIMISATION PROCEDURE

The optimizations have been performed using DLR's optimization tool *AutoOpti*. *AutoOpti* is an automated optimization tool based on an evolutionary algorithm, coupled with response surface technologies such as Kriging and artificial neural networks. It is capable of multi-objective optimizations. Details regarding *AutoOpti* can be found in Voß [4] and Siller [5]. *AutoOpti* allows to specify arbitrary process chains which will be sequentially processed for each member during the optimization. The process chain used for the optimizations consists of the fol-

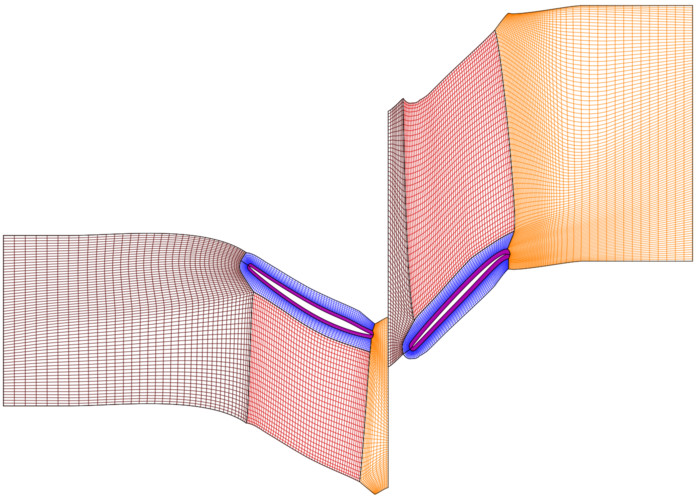

FIGURE 3. COMPUTATIONAL GRID.

TABLE 2. MAIN OPTIMISATION PARAMETERS

Parameter		Min	Max
R1 stagger angle [°]	$\beta_{S.\mathrm{R1}}$	105	125
R1 LE angle [°]	$\beta_{1.\mathrm{R1}}$	115	130
R1 TE angle [°]	$\beta_{2.\mathrm{R1}}$	85	100
R1 rel. LE radius [-]	$r_{LE.\mathrm{R1}}/c_{R1}$	0.003	0.008
R1 rel. max. thickness [-]	$D_{\max.\mathrm{R1}}/c_{R1}$	0.04	0.08
R1 rel. pos. max. thick. [-]	$x_{D\max.\mathrm{R1}}/c_{R1}$	0.4	0.75
R2 stagger angle [°]	$\beta_{S.\mathrm{R2}}$	115	135
R2 LE angle [°]	$\beta_{1.\mathrm{R2}}$	120	138
R2 TE angle [°]	$\beta_{2.\mathrm{R2}}$	94	114
R2 rel. LE radius [-]	$r_{LE.\mathrm{R2}}/c_{R2}$	0.003	0.006
R2 rel. max. thickness [-]	$D_{\max.\mathrm{R2}}/c_{R2}$	0.03	0.05
R2 rel. pos. max. thick. [-]	$x_{D\max.\mathrm{R2}}/c_{R2}$	0.4	0.7

lowing successive steps:

1. Geometry generation of rotor one and rotor two
2. Grid generation
3. CFD simulation with automatic convergence control
4. Calculation of fitness function values

The operating point for the optimizations is a cruise design point, defined by the following properties:

Total pressure at inlet $p_{t.in}$ = 35500Pa
Total temperature at inlet $T_{t.in}$ = 245.5K
Total pressure ratio Π_{tot} = 1.3

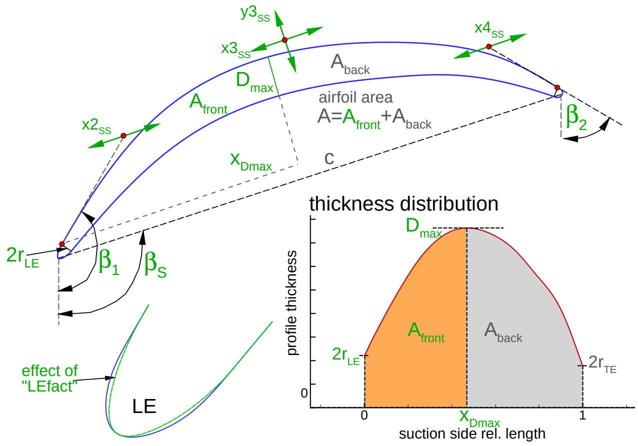

FIGURE 4. AIRFOIL PARAMETERIZATION.

The total pressure ratio is the result of a preliminary design study which has been conducted prior to the optimizations and is not part of the present study. By means of the preliminary study the optimal stage pressure ratio as well as an optimal total mass flow through the stage have been identified and used as boundary conditions for the optimization setup. In general, the overall aim of an optimimzation with a setup similar to the one presented here, would be to find a good trade-off between fan size and efficiency. Therefore two fitness functions were defined, aiming at maximising the isentropic efficiency and the mass flow rate of the configuration at the defined operating point:

$$f_1 = \eta_{is} \quad (1)$$
$$f_2 = \dot{m} \quad (2)$$

As the stream tube which has been used for the optimizations is constant for all members, a member achieving a high mass flow rate also has a high flow density. For a given total mass flow rate through the fan, a member with a higher mass flow rate through the stream tube considered during the optimization would result in a fan with a smaller fan diameter. Hence, the second fitness function is a measure to reduce the fan diameter.

To keep the total pressure ratio of $\Pi_{tot} = 1.3$ constant for all members during the optimizations a PID controller has been used for the *TRACE* simulations. The PID controller is coupled with the CFD solver in an in-line fashion and is adjusting the static pressure at the outlet boundary during the CFD simulations, so that the desired pressure ratio is achieved. During convergence the pressure adjustment reaches a constant value. The PID controller has no influence on the results obtained.

The swirl at the exit of rotor 2 has been restricted by means of restricting the outlet flow angle of rotor 2 to vary within $\beta = 0^\circ \pm 5^\circ$ only. Members which did not comply with the restriction

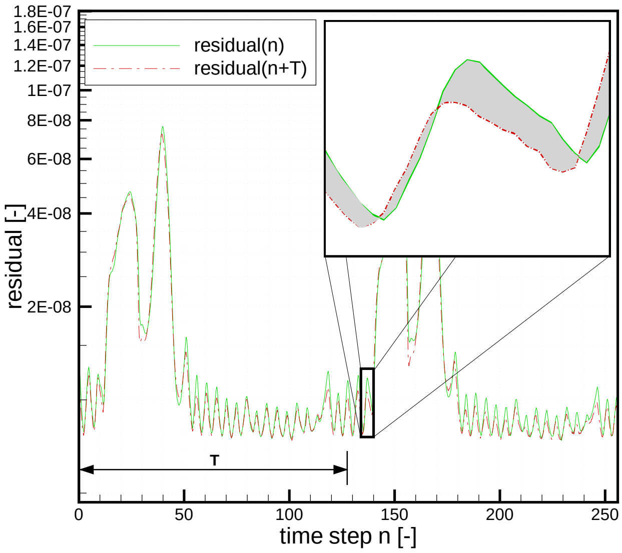

FIGURE 5. PERIODIC DIFFERENCE. Plot of the density residual over the time steps of the actual quantity and shifted by one period T.

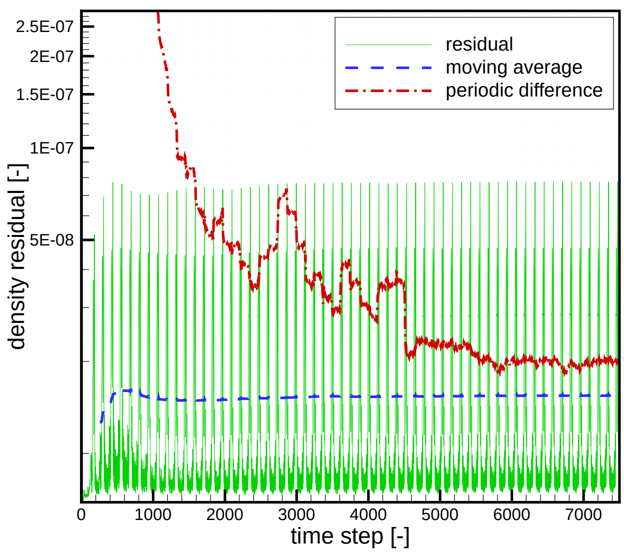

FIGURE 6. PERIODIC DIFFERENCE AND MOVING AVERAGE.

were penalized during the optimization. This was necessary, as the efficiency is calculated based on mixed-out flow properties at the boundaries and does not account for additional losses by swirl left in the flow. An outlet flow angle of $\beta = 5°$ leads to a drop in efficiency of approximately 1%.

Convergence control for optimizations based on unsteady CFD

In order to perform an optimization based on unsteady CFD the convergence control tool of *AutoOpti* had to be extended. As unsteady simulations have periodically changing output values, not the instantaneous value at a current time step is used to determine the state of convergence, but instead the values over one period are evaluated. The length of the period used for evaluation is defined by the blade passing frequency which is expected to be equal to the frequency of the most significant unsteady fluctuations. An overview of the topic of convergence prediction in periodic-unsteady flow fields is given in Clark [6].

For the present study a simple criterion based on the comparison of two consecutive periods has been established, integrating the absolute value of the difference of the two periods:

$$\Delta_t = \int_{t-T}^{t} |y(\tau) - y(\tau - T)| \, d\tau \tag{3}$$

Or, for discrete time steps, as a sum over the differences (as shown in figure 5):

$$\Delta_n = \sum_{l=n-N+1}^{n} |y_l - y_{l-N}| \tag{4}$$

Where n are the time steps and N the time steps per period, which are known as they are an input value for the solver settings. For the current study a value of N=128 time steps per period with 20 sub iterations has been used.

Figure 6 shows exemplarily a comparison of the moving average (average value over the interval $[n-N+1;n]$ at each time step n) and the periodic difference Δ_n of an unsteady simulation for the density residual. Using the periodic difference allows a much more accurate automated prediction of the state of convergence.

The automated convergence control tool checks for defined quantities, such as residual and mass flow rate, if the value of the quantity or, in the case of unsteady simulations, the periodic difference of the value fulfils certain criteria. Criteria applicable are a maximum or minimum value and an allowed degree of variation of the value. The chosen criteria must hold over a defined number of time steps before the simulation is regarded as converged.

Deterministic stress approach

Modelling deterministic stresses is an approach to combine the advantages of steady state and time-accurate simulation procedures, namely low computational cost and high physical accuracy. The deterministic stresses reproduce the effect of unsteadiness on the time-averaged solution and therefore improve the solution of the steady flow field without the need of a time-accurate computation.

The employed methodology is based on the average-passage equation system established by Adamczyk [7]. The key idea of the present approach is to correlate the additional deterministic stress terms τ_{ij}^{det} with the local strain rate:

$$\tau_{ij}^{det} = \overline{\overline{\rho u_i'' u_i''}} = \mu_d \cdot \left(\frac{\partial u_i}{\partial x_j} + \frac{\partial u_j}{\partial x_i} \right) \tag{5}$$

This approach is analogous to Boussinesq's approximation but leaving out the pressure term. In order to model the deterministic stresses, one additional transport equation needs to be solved. More details are given in Stollenwerk [8].

OPTIMIZATION RESULTS

Firstly the results of the optimizations for configuration one (high axial spacing) are presented to demonstrate the validity and appropriate implementation of the tools for unsteady optimization and convergence control. Thereafter, the results of the optimizations of configuration two are presented to analyse under what circumstances steady state and unsteady CFD methods can yield different results when applied in the framework of optimizations. Finally, the results of a optimization incorporating a deterministic stresses approach are discussed.

Validation of the process chain for optimizations based on unsteady CFD

The first configuration with high axial spacing was used to validate the process chain and optimization tools for unsteady optimizations. Due to the high axial spacing the unsteady interaction of the flow past the two rotors is low. Therefore it was expected to get the same results independent of the type of CFD method used, steady state or unsteady. Two optimizations were conducted. One based on steady state, the other on unsteady CFD, referred to in the following as “steady state optimization” (SSO) and “unsteady optimization” (USO), respectively. Prior to the optimizations a design of experiments (DOE) was carried out to provide a set of 500 members that cover the whole design space. These members were used as starting members for both optimizations, in order to have equal starting conditions.

The Pareto fronts of the two optimizations are shown in figure 7. The unsteady optimization was stopped at a slightly earlier stage of convergence which explains the not so smooth Pareto front. Despite this it can be concluded that both optimizations yield the same results. To underline this statement the Pareto front members of the steady optimization have been recalculated using unsteady CFD (see figure 7) and vice versa. The two results (using steady and unsteady CFD) of each member showed only minor offsets with slightly better results using steady CFD. It can be reasoned that for this configuration with high axial spacing the optimization result is independent of the CFD method used. This can be seen as a validation of the unsteady optimization tools, including the convergence control tool for unsteady CFD. Furthermore it can be concluded that for cases where a low unsteady interaction between the blade rows for all possible members free to be generated during the optimization can be expected, a steady state optimization is sufficient.

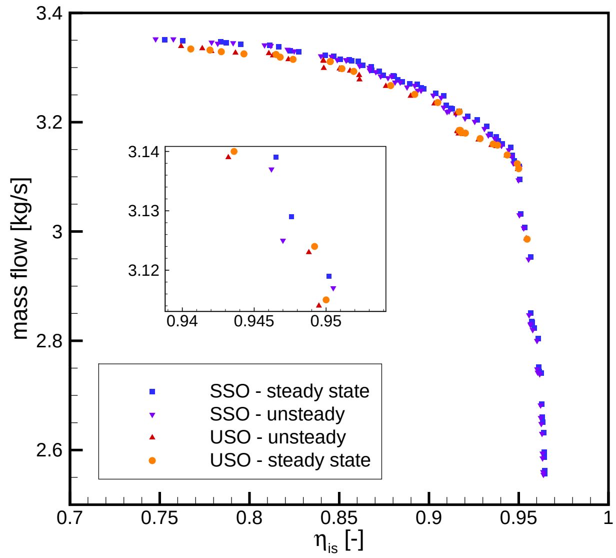

FIGURE 7. CONFIGURATION 1 PARETO FRONTS OF STEADY AND UNSTEADY OPTIMIZATION AND RECALCULATIONS.

Differences between optimizations based on steady and unsteady CFD for significant unsteady interaction

For the second configuration, again two optimizations (steady state and unsteady) have been conducted under equal conditions and with the same starting members obtained by the DOE. The resulting Pareto fronts (see figure 8) show a more distinct difference than the ones obtained with configuration one. The steady state optimization predicts better results than the unsteady optimization.

When recalculating the Pareto front members with the other method, i.e. recalculating the steady optimization Pareto front members using unsteady CFD and the unsteady optimization Pareto front members using steady CFD, the results do not match over the whole Pareto front, as they do for configuration one.

Instead, the Pareto front can be divided into two parts. Only for mass flow rates of approximately $\dot{m} \lessapprox 2.9 \frac{kg}{s}$ ($\mathrm{Ma}_{ax} \lessapprox 0.6$) the steady Pareto front can be converted into the unsteady Pareto front when recalculating the Pareto front members using URANS and the other way round.

Consequently for this part of the Pareto front the optimization result is more or less independent of the CFD method, although the absolute values of the fitness functions differ depending on the CFD method used. But for the part of the Pareto front that is, in terms of optimization goals, the most important, namely the part showing high values of both fitness functions, the optimization results clearly depend on the CFD method used.

Presuming an unsteady CFD simulation provides results with higher accuracy compared to a steady simulation, the quality of both optimizations can be compared when recalculating the steady optimization results using unsteady CFD. The comparison of these recalculated members with the Pareto front members of the unsteady optimization shows that using unsteady CFD during the optimization, in this case, yields better results in terms of fitness function values (see figure 8).

A significant disagreement between the predicted fitness function values of the steady optimized members and the unsteady recalculated members can be observed. Furthermore the disagreement varies depending on the member. On the other hand the comparison of the unsteady optimization Pareto front members with the results of a recalculation of the same members using steady CFD shows a much lower difference in fitness value prediction.

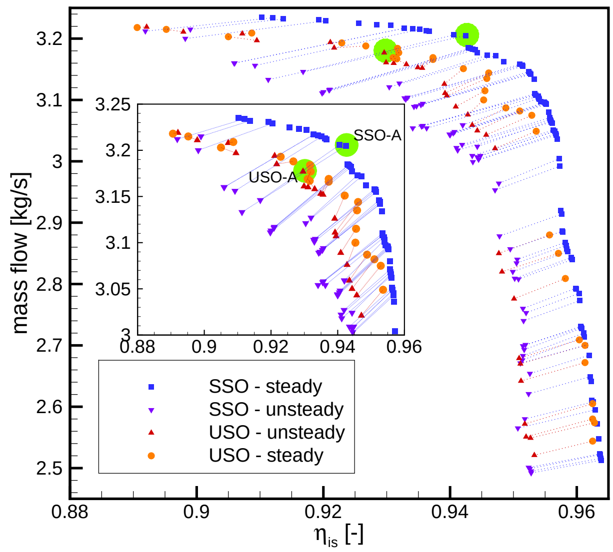

FIGURE 8. CONFIGURATION 2 PARETO FRONTS OF STEADY AND UNSTEADY OPTIMIZATION AND RECALCULATIONS.

Optimising based on a solver using a deterministic stresses approach

Modelling deterministic stresses aims at reproducing the effects of unsteady flow phenomena on the time averaged solution. Using a CFD solver that incorporates such a model in the framework of optimizations promises to produce results that do not suffer from such high inaccuracy in the prediction of the fitness values as has been observed using a steady CFD solver. An optimization has been performed for configuration two based on a RANS solver that includes a model for the deterministic stresses (referred to in the following as "DS optimization"). All other settings were identical to the prior optimizations with the exception that for this optimization the fitness functions have been restricted to values of $\dot{m} > 3$ and $\eta_{is} > 0.89$ to focus on the area of the Pareto front which showed the largest differences between the results of the optimization based on the steady CFD solver and the time-accurate recalculations. The resulting Pareto front is shown in figure 9. The Pareto front members of the DS optimization have been recalculated using a time-accurate solver, as was done for the prior optimizations. Comparing the unsteady recalculations of the Pareto front members of the DS optimization and the steady optimization as well as the Pareto front members of the unsteady optimization shows the performance of the DS model. Although the results of the unsteady optimization are still not reached in terms of fitness function, an overall improvement compared to the SSO can be observed. Hence, compared to the SSO a DS optimization shows better results with the same computing power needed.

Computational cost of the optimizations

For the sake of completeness some comments are given on the computational cost of the different optimizations. For this study all optimizations were left to reach a good state of convergence, as the best possible solutions of the optimizations should be compared. The state of convergence can be judged by the improvement of the Pareto front over the number of evaluations. As a URANS simulation needs around ten times the computing cost of a RANS or RANS-DS simulation, the USOs were stopped, as soon as the tendency became clear, whereas the SSOs and DSO were left running for some more time. Nevertheless it has been made sure that even the USO reached a state of convergence where no additional significant improvement can be expected. The main difference are the smoother Pareto fronts of the SSOs and DSO. This also reflects, up to a certain degree, the typical situation where the computational resources are limited and can either be used to compute a large number of low fidelity members or low number of high fidelity members. In total the SSOs

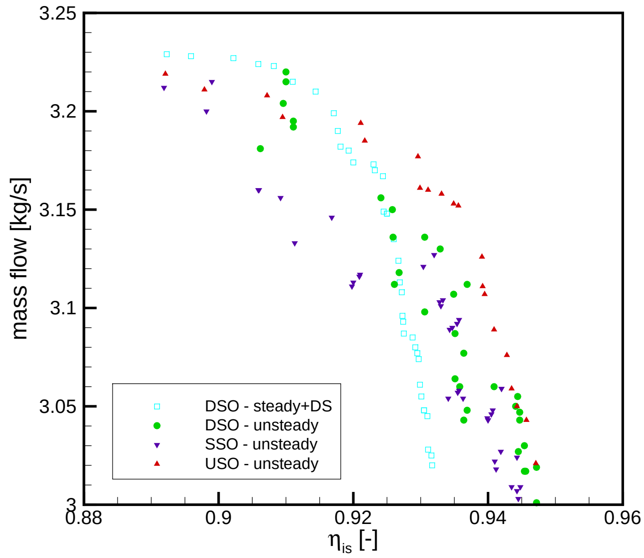

FIGURE 9. CONFIGURATION 2 PARETO FRONTS

both reached approximately 10000 converged members, whereas the USOs reached around 2500 converged members. The DSO reached 3000 converged members. In average 20% of the members did not complete the process chain successfully.

AERODYNAMIC ANALYSIS

The results that have been obtained by the different optimizations show how using a steady CFD method within an optimization can yield in fitness function predictions that can not be met when recalculating the same members using a time-accurate solver.

In order to understand the cause for the difference in the results of the steady and unsteady optimizations of configuration two, two members have been analysed in detail. The first member, referred to as SSO-A, is a member of the Pareto front of the SSO. It shows a clear difference regarding the two fitness function between its steady solution and an unsteady recalculation. The second member, referred to as USO-A, is a member of the Pareto front of the USO and does show only a slight difference between its unsteady and steady solution. The fitness functions of the two members obtained by the different CFD methods for the operating point of the optimization are listed in table 3 and highlighted in figure 8.

Comparing the steady state solution of member SSO-A shown in figure 12(a) with the time average of the unsteady solution shown in figure 12(c) a different flow picture can be observed. The solution of the unsteady simulation shows a more

TABLE 3. Fitness function values obtained using steady (SS) and unsteady (US) CFD of selected members of configuration two, optimised using steady CFD (SSO) or unsteady CFD (USO).

	steady CFD		unsteady CFD		difference	
Member	$f_{1.SS}$	$f_{2.SS}$	$f_{1.US}$	$f_{2.US}$	Δ_{f_1}	Δ_{f_2}
SSO-A	0.942	3.205	0.911	3.133	0.031	0.072
USO-A	0.932	3.184	0.930	3.177	0.002	0.007

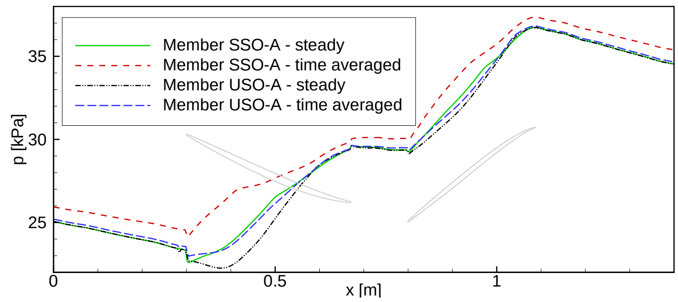

FIGURE 10. PITCHWISE AVERAGED PRESSURE OF MEMBER SSO-A AND USO-A FOR STEADY AND UNSTEADY CALCULATIONS.

upstream position of the shocks on both rotors. Furthermore the shocks are sharper. When analysing the circumferentially averaged value of the pressure along the machine axis it can be observed that for the unsteady simulation the pressure is approximately 700Pa higher throughout the machine compared to the steady solution (see figure 10). As the total pressure ratio has been kept constant ($\Pi_{tot} = 1.3$) for all the calculations using a PID controller as described above, it can be concluded, as expected [9] [10], that the unsteady simulation predicts higher losses than the steady simulation does. In order to reach the defined total pressure ratio the stage has to be throttled to a higher back pressure. As a consequence the mass flow rate and the axial velocity are reduced (see figure 11). Thus the flow angles and the incidences at the rotors change. These effects result in the different shock positions and the different flow pattern observed and hence in the different fitness function values.

When comparing the steady (figure 12(b)) and time averaged (figure 12(d)) flow fields of member USO-A, an equal but less distinct tendency can be observed between the steady and unsteady simulation. Again the losses predicted by the unsteady simulation are slightly higher, but as the member has been optimized using unsteady CFD all unsteady effects that result in higher losses have been taken into account during the optimization process and have been minimized. The result is rotor two operating at an unthrottled state (see figure 11) with a reduced shock close to the trailing edge. Therefore the upstream effect of

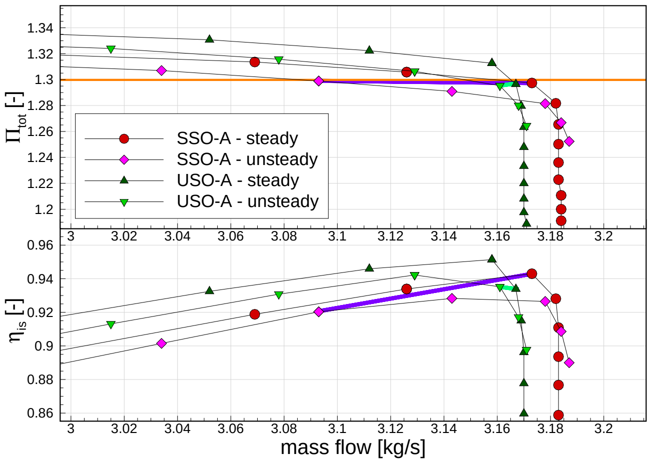

FIGURE 11. SPEEDLINES OF MEMBER SSO-A AND USO-A FOR STEADY AND UNSTEADY CALCULATIONS.

the shock is much lower compared to that of member SSO-A.

The upstream effect of the shock at rotor two can be seen in figures 13(a) and 13(b). Plotted is a pressure contour of a quarter perimeter of the machine. A field of locally high pressure travelling in upstream direction can be observed for both members. This field of high pressure is travelling along the pressure side of rotor one and is also influencing the shock at the suction side of rotor one. The interference with the shock is stronger for member SSO-A.

This difference in the flow interaction of the two rotors and especially the upstream effect of the shock at rotor two that can be observed for the two members is characterising the two optimizations (SSO/USO) of configuration two.

The USO procedure has taken into account all unsteady effects and the flow interaction between the rotors for the defined OP has been minimized. Therefore the difference Δ_f between the results of the unsteady and the steady simulation of the unsteady optimized members is low.

For the SSO the interaction was not reproduced by the CFD simulation, as the steady simulations during the SSO were done with a “mixing plane”-interface between the two rotors, which involves a pitchwise averaging process of the flow. This simplification yields to an additional uncertainty in the estimation of the global performance parameters and thus in the calculation of the fitness function values. As a result other geometries have been identified as Pareto-rank one members in the SSO.

CONCLUSION AND OUTLOOK

An investigation has been conducted into the dependency of optimization results on the CFD method used within the optimization procedure. Two configurations of a Q3D counter rotating fan configuration with different axial spacing have been optimized, both using steady state and unsteady CFD. In addition, the configuration with lower axial spacing has been optimized using a steady state solver with an incorporated deterministic stresses model.

It has been shown that an increased uncertainty of the steady state CFD in calculating the global values due to high unsteady interaction can lead to different optimization results of a SSO compared to an USO. Whilst for the configuration with high axial spacing and hence low unsteady interaction no benefit in using an unsteady method during the optimization could be observed, the optimizations of the configuration with low axial spacing showed different results for the optimizations based on steady state and unsteady CFD. This has resulted in Pareto optimal members of the SSO that show, when being recalculated with the unsteady solver, less good results in terms of fitness function values compared to the Pareto optimal members of the USO. The benefit in using the unsteady solver has been observed for axial Machnumbers of $\mathrm{Ma}_{ax} \gtrsim 0.6$. Incorporating a deterministic stresses model, better results compared to the SSO could be obtained but still not as good as obtained by the USO procedure.

It can be concluded that optimizations based on unsteady CFD can lead to better results compared to optimizations based on steady CFD. This is especially the case for configurations and operating points with high unsteady interaction. For configurations with low unsteady interaction a steady state CFD solver can be sufficient.

As unsteady CFD is more costly in terms of computational power, a practicable approach to optimization problems is, to start with an optimization based on a steady CFD solver and to use the optimized members of the SSO as starting members of a subsequent USO.

Future work might focus on developing multi-fidelity optimization procedures that combine multiple CFD methods and minimize the use of costly unsteady CFD.

ACKNOWLEDGMENT

The investigations were conducted as part of the joint research programme COORETEC-turbo in the frame of AG Turbo. The work was supported by the Bundesministerium für Wirtschaft und Technologie (BMWi) as per resolution of the German Federal Parliament under grant number 0327717C. The authors gratefully acknowledge AG Turbo for their support and permission to publish this paper. The responsibility for the content lies solely with its authors.

REFERENCES

[1] Lott, P. T., Hills, N. J., Chew, J. W., Scanlon, T., and Shahpar, S., 2009. “High pressure turbine stage endwall profile optimisation for performance and rim seal effectiveness”.

In Proceedings of ASME Turbo Expo 2009, no. GT2009-59923, pp. 1075–1087.

[2] Ashcroft, G., Heitkamp, K., and Kügeler, E., 2010. "High-order accurate implicit runge-kutta schemes for the simulation of unsteady flow phenomena in turbomachinery". In Proceedings of the 5th European Conference on Computational Fuild Dynamics ECCOMAS CFD, Lisbon, Portugal.

[3] Becker, K., Heitkamp, K., and Kügeler, E., 2010. "Recent progress in a hybrid-grid CFD solver for turbomachinery flows". In Proceedings of the 5th European Conference on Computational Fuild Dynamics ECCOMAS CFD, Lisbon, Portugal.

[4] Voß, C., Aulich, M., Kaplan, B., and Nicke, E., 2006. "Automated multiobjective optimization in axial compressor blade design". In Proceedings of ASME Turbo Expo 2006, Barcelona, Spain, no. GT2009-59923.

[5] Siller, U., Voß, C., and Nicke, E., 2009. "Automated multidisciplinary optimization of a transonic axial compressor". In Proceedings of the 47th AIAA Aerospace Sciences Meeting Including the New Horizons Forum and Aerospace Exposition.

[6] Clark, J. P., and Grover, E. A., 2007. "Assessing convergence in predictions of periodic-unsteady flowfields". *Journal of Turbomachinery,* ***129***(4), pp. 740–749.

[7] Adamczyk, J. J., 1985. "Model equation for simulating flows in multistage turbomachinery". In *ASME Paper*, no. 85-GT226.

[8] Stollenwerk, S., and Nürnberger, D., 2009. "A model for potential deterministic effects in transonic compressor flows". In Proceedings of ASME Turbo Expo 2009, Orlando, Florida, USA, no. GT2009-60105.

[9] Denton, J. D., 2010. "Some limitations of turbomachinery CFD". In Proceedings of ASME Turbo Expo 2010, Glasgow, UK, no. GT2010-22540.

[10] Praisner, T. J., Clark, J. P., Nash, T. C., Rice, M. J., and Grover, E. A., 2006. "Performance impacts due to wake mixing in axial-flow turbomachinery". In Proceedings of ASME Turbo Expo 2006, Barcelona, Spain, no. GT2006-90666.

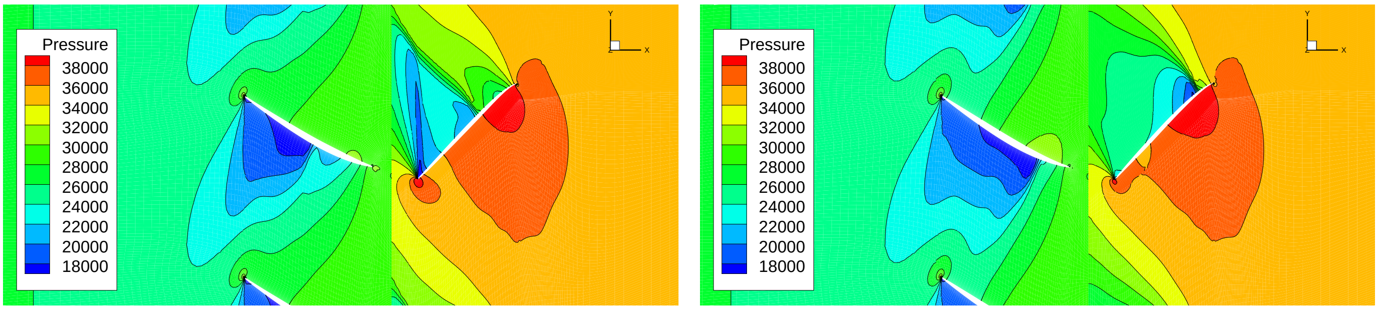

(a) Member SSO-A - RANS calculation

(b) Member USO-A - RANS calculation

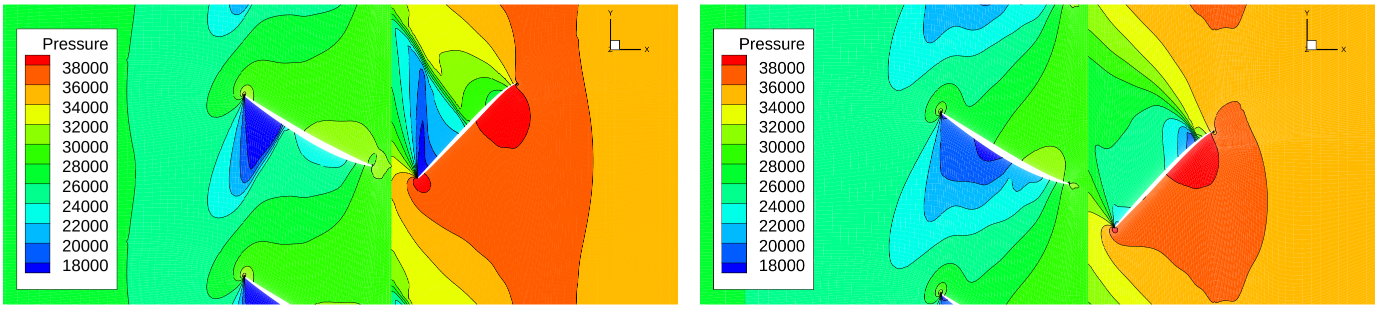

(c) Member SSO-A - time averaged URANS calculation

(d) Member USO-A - time averaged URANS calculation

FIGURE 12. Pressure contour plots of member SSO-A and USO-A

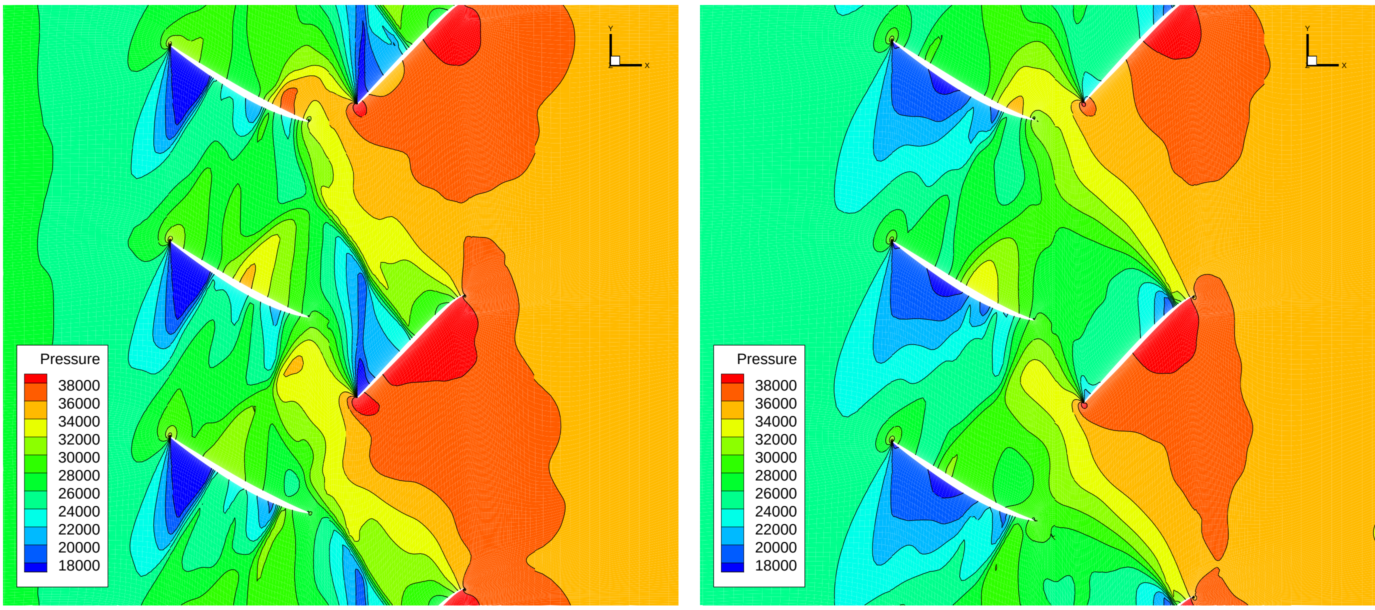

(a) Member SSO-A

(b) Member USO-A

FIGURE 13. Snapshot of Pressure Contour Plots of URANS calculation